Applied Physics Letters

# Nonlinear frequency conversion of vectorial optical fields with a Mach-Zehnder interferometer

Cite as: Appl. Phys. Lett. **114**, 241901 (2019); https://doi.org/10.1063/1.5095864
Submitted: 13 March 2019 . Accepted: 05 June 2019 . Published Online: 18 June 2019

Hui Li, Haigang Liu, and Xianfeng Chen

Applied Physics Letters ARTICLE scitation.org/journal/apl

# Nonlinear frequency conversion of vectorial optical fields with a Mach-Zehnder interferometer

Cite as: Appl. Phys. Lett. **114**, 241901 (2019); doi: 10.1063/1.5095864
Submitted: 13 March 2019 · Accepted: 5 June 2019 ·
Published Online: 18 June 2019



Hui Li,[1,2] Haigang Liu,[1,2,a)] and Xianfeng Chen[1,2,b)]

## AFFILIATIONS

[1]State Key Laboratory of Advanced Optical Communication Systems and Networks, School of Physics and Astronomy, Shanghai Jiao Tong University, Shanghai 200240, China
[2]Key Laboratory for Laser Plasma (Ministry of Education), Collaborative Innovation Center of IFSA (CICIFSA), Shanghai Jiao Tong University, Shanghai 200240, China

[a)]Electronic mail: liuhaigang@sjtu.edu.cn
[b)]Electronic mail: xfchen@sjtu.edu.cn

## ABSTRACT

Vectorial optical fields with inhomogeneous polarization states have attracted great interest for their unique properties in both quantum and classical physics. In this paper, we propose a method to realize such nonlinear frequency conversion of the vectorial optical fields, which is by using a Mach–Zehnder interferometer. The separated arms enable two nonlinear processes to simultaneously proceed in two vertical directions. In our experiment, nonlinear frequency conversion of fundamental frequency vectorial optical fields with topological charge $l = 3$ is studied. To illustrate the flexibility of this method, Taiji and clover patterns with inhomogeneous polarization distribution are also generated at second harmonic wavelengths. This research proposes a more flexible method to realize nonlinear frequency conversion of the vectorial optical fields and may have potential applications in the generation of ultrafast vectorial optical fields.



It is well known that polarization is an important parameter to characterize the properties of light beams. Previous research studies mainly focus on homogeneous polarization beams, such as linear, elliptical, or circular polarization beams. It was until 1961 that Snitzer put forward the concept of the vectorial optical field.[1] Prominent examples of vectorial optical fields are radially polarized and azimuthally polarized beams. In 1972, Mushiake *et al.* first verified the generation of radially polarized beams by using laser oscillation.[2] Almost at the same time, Pohl proved that azimuthally polarized optical beams could be output by operating a ruby laser.[3] Recent studies have shown that the electric field of the radially polarized optical beam can be focused to a strong longitudinal field near the focus of the objective,[4–6] and the azimuthally polarized beam can be used to create a strong longitudinal magnetic field.[7] Of particular interest in those properties, vectorial optical fields have attracted great interest for their potential applications in various research fields, such as laser micromachining,[8,9] optical trapping,[10,11] microscopy,[12,13] optical cages,[14,15] and so on. In the field of laser micromachining, the morphology of the boreholes induced by radially polarized femtosecond laser pulses is obviously smoother and better-delineated compared to those produced by circularly and linearly polarized pulses.[8] Vectorial optical fields are also used to enhance the sensitivity of nonlinear microscopy because the nonlinear process is strongly affected by the polarization of the incident beams.[16] Besides, vectorial optical fields have sparked great interest for their broad application in the fields of high resolution imaging[17] and optical micromanipulation.[10,18] Until now, a variety of methods have been proposed to generate the vectorial optical fields. One method is by utilizing a fiber laser incorporated with proper fiber grating to generate vectorial optical fields.[19] Another method is to use a digital micromirror device (DMD) to accurately manipulate the optical field with a specified pattern.[20] Besides, metasurfaces,[21,22] photoalignment liquid crystals,[23] q-plates,[24,25] and spatial light modulators[26–28] (SLMs) have also been applied to produce vectorial optical fields. However, the research studies mentioned above are all carried out in the linear optical realm.[21–28] In our previous research, we propose the nonlinear frequency conversion of such vectorial optical fields by using cascading nonlinear crystals.[29] Recently, the nonlinear frequency conversion of such vectorial optical fields has also been realized in a Sagnac loop.[30]

Here, in this paper, we propose a method to realize such nonlinear frequency conversion of the vectorial optical fields, which is by using a Mach–Zehnder interferometer. The two arms of the

Mach–Zehnder interferometer enable nonlinear frequency conversion of the horizontal and vertical polarizations of the vectorial optical fields at the same time. In our experiment, nonlinear frequency conversion of fundamental frequency (FF) vectorial optical fields with topological charge $l = 3$ is studied, and the vector properties are measured by employing a Glan-Taylor prism. In addition, to illustrate the flexibility of the method proposed here, nonlinear Taiji and clover patterns with different polarization states are also realized.

The experimental setup is illustrated in Fig. 1. The Jones vector field of the incident FF vectorial optical field can be expressed as $E(\omega) = [\cos(l\varphi + \varphi_0), \sin(l\varphi + \varphi_0)]$ in which $l$ represents the topological charge of the fundamental wave and $\varphi$ is the azimuth angle. $\varphi_0$ refers to the initial phase. Figure 1(a) shows the polarization and intensity distribution of the FF vectorial optical field with the topological charge $l = 3$. Two 4-f systems (consisting of lenses $L_1$ and $L_2$ and lenses $L_1$ and $L_3$) are used to imprint the FF wave on two samples ($S_1$ and $S_2$). $BS_1$ is used to separate the FF vectorial optical field into two parts. Two separated beams are propagated through the 1 mm thick samples, respectively. Both samples are homogenous 5-mol. % MgO:$LiNbO_3$ crystals and they are placed in two orthogonal directions. Two separated samples in the arm of the Mach–Zehnder interferometer satisfy the type-I (oo-e) phase matching condition to generate SH vectorial optical fields. The angle between the propagation direction and optical axis of the crystal is 75° on the basis of the Sellmeier equation.[31] The generated nonlinear beams are recombined with $BS_2$. To improve the utilization of the FF vectorial optical field, two BSs can be changed into polarized BSs. Lenses $L_4$ and $L_5$ with a focal length of 100 mm are used to image the generated nonlinear vectorial optical field onto a charge coupled device (CCD). To characterize and validate the vector properties of the generated SH vectorial optical field, a GT prism is used. At last, a filter (F) in front of the CCD can be used to filter out the FF vectorial optical field. It should be pointed out that Mach–Zehnder interferometers have many advantages compared to the previous configurations.[29,30] First, the nonlinear crystals can be individually adjusted in two separated arms of the Mach–Zehnder interferometer. Therefore, the two samples are easier to adjust to satisfy the phase matching condition. Second, the diffraction effect can be suppressed to some extent compared to Ref. 29 as

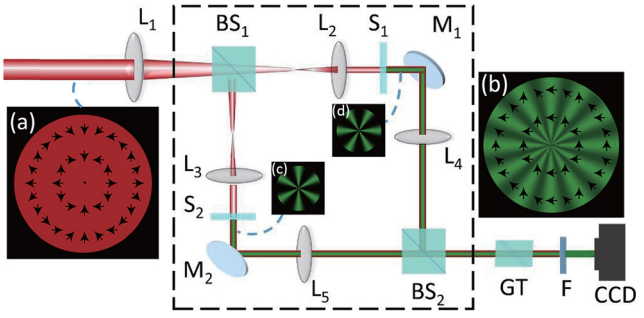


**FIG. 1.** Schematic of the experimental setup. Focal length $L_{1,\ldots,5}$ = 200 mm, 50 mm, 50 mm, 100 mm, and 100 mm, respectively; BS: beam splitter; $S_1$ and $S_2$: 5-mol. % MgO:$LiNbO_3$; $M_1$ and $M_2$: mirrors; GT prism: Glan-Taylor prism; F: filter; CCD: charge coupled device. (a) The polarization and intensity distribution of the FF vectorial optical field. (b) The polarization and intensity distribution of the generated second harmonic (SH) vectorial optical field. (c) and (d) The spatial intensity distribution of the generated SH beam in two arms.

the relative positions of two nonlinear crystals can be flexibly adjusted. Besides, compared to Ref. 30, our method shows its powerful controllability to the local polarization states of the generated nonlinear vectorial optical fields.

The FF vectorial optical field corresponding to the upper arm of the Mach–Zehnder interferometer, which incidents onto $S_1$, satisfies the phase matching condition. Supposing the light propagates along the z-axis, under the undepleted-pump and paraxial approximation, the coupled wave equation of the SH optical field can be written as

$$\frac{dE_{SH1}(2\omega)}{dz} = A_0 E_h(\omega) E_h(\omega), \tag{1}$$

where $E_{SH1}(2\omega)$ is the generated SH field, $A_0$ is a parameter that characterizes the strength of the nonlinearity, and $E_h(\omega)$ represents the horizontal component of the FF vectorial optical field. As a result, the optical field of the generated SH can be written as $E_{SH1} = A_0 L[0, \cos^2(l\varphi + \varphi_0)]$, where $L$ refers to the length of the nonlinear crystal along the propagation direction of light. The intensity is theoretically depicted in Fig. 1(d). Similarly, the optical field of the generated SH in another arm can be written as $E_{SH2} = A_0 L[\sin^2(l\varphi + \varphi_0), 0]$. Figure 1(c) shows the intensity distribution of the corresponding SH field in theory. As a result, the final output field of the upper arm is given by $E_{SHR} = E_{refl} E_{refl} E_{SH1} = A_0 L[0, \cos^2(l\varphi + \varphi_0)]$, where $E_{\text{refl}} = \begin{pmatrix} -1 & 0 \\ 0 & 1 \end{pmatrix}$. Similarly, the lower one can be represented as $E_{SHL} = A_0 L[-\sin^2(l\varphi + \varphi_0), 0]$. At last, the Jones vector field of the final generated SH vectorial optical field can be expressed in the form

$$E_{SH}(2\omega) = A_0 L\left[-\sin^2(l\varphi + \varphi_0), \cos^2(l\varphi + \varphi_0)\right]. \tag{2}$$

The polarization distribution of the generated SH vectorial optical field can be influenced by $\varphi_0$. Without loss of generality, we set that $\varphi_0 = 0$ in all cases. As a result, the Jones vector field of the generated SH vectorial optical field can be expressed as $E_{SH}(2\omega) = A_0 L[-\sin^2(l\varphi), \cos^2(l\varphi)]$. Theoretically, the intensity and polarization distribution of the generated SH vectorial optical field are displayed in Fig. 1(b).

First, we examine the frequency conversion of the FF vectorial optical field with topological charge $l = 3$. Figures 2(a) and 2(b) show the simulated intensity and polarization distribution corresponding to the FF vectorial optical field and the generated SH vectorial optical field, respectively. Figures 2(c1) and 2(d1) describe the intensity distribution of the generated SH vectorial optical field in simulated and experimental environments, respectively. To validate the polarization properties of the cross section of the SH vectorial optical field, a GT prism is used. By passing through the GT prism, as shown in Fig. 1, with different polarization angles 0°, 40°, 80°, 100°, 130°, 150°, 170° with respect to the positive horizontal direction, the simulated and experimental intensity distributions of the generated SH vectorial optical fields are shown in Figs. 2(c2)–2(c8) and Figs. 2(d2)–2(d8), respectively. The observed patterns in Figs. 2(c1) and 2(d1) are split into six lobes displayed in Figs. 2(c2) and 2(d2), while the polarization direction of the GT prism has a polarization angle of 0°. In this situation, the generated SH vectorial optical field in the 0°, 60°, 120° directions of the cross section is perpendicular to the polarization direction of the GT prism. It is interesting that as the GT prism rotated to 40°, one can find that the extinction direction altered and increased to 14°, 44°, 74°, 104°, 134°, 164° for components perpendicular to the axis of the

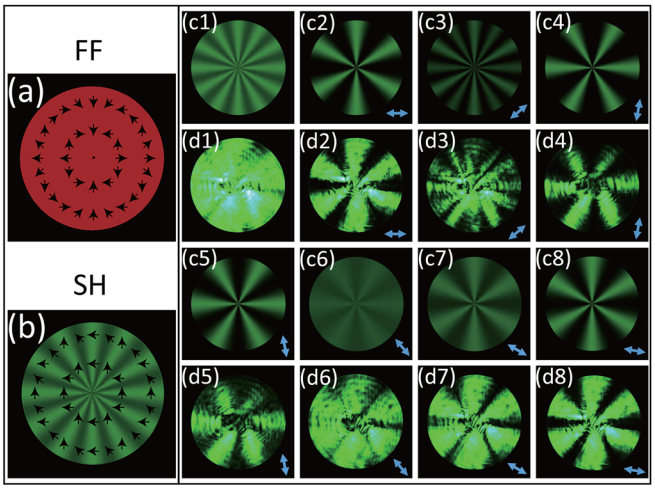


**FIG. 2.** (a) and (b) Show simulated intensity and polarization distribution of the FF vectorial optical field with topological charge $l = 3$ and the generated SH vectorial optical field, respectively. (c1)–(c8) Simulated intensity profile of the SH vectorial optical field without a GT prism and when the GT prism has different polarization angles ($0°, 40°, 80°, 100°, 130°, 150°, 170°$) with respect to the positive horizontal direction. (d1)–(d8) Show the corresponding experimental results.

GT prism increased. However, the extinction direction returns to three when the polarization angle is 80°, as shown in Figs. 2(c4) and 2(d4). Note that when the polarization angle increased from 80° to 100°, six lobes get broader for components parallel to the axis of the GT prism increase. An amazing phenomenon is that the intensity is almost homogeneous distribution in Figs. 2(c6) and 2(d6), which is attributed to the fact that no polarization state of the whole vector is strictly perpendicular to the polarization direction of the GT prism. As the GT prism rotates from 130° to 170°, six petals come into being and become more and more obvious. It is noticeable that Fig. 2(c1) is the sum of Figs. 2(c4) and 2(c8). Such an intensity changing trend is almost the contrary process compared with our previous research[29] because of the polarization difference of the generated SH vectorial optical fields in these two methods. We measure the intensity of the FF and SH vectorial fields corresponding to 10.7 mW and 14.4 $\mu$W, respectively. As a result, the SH efficiency is approximately 1.35‰.

A Taiji pattern with two vertical polarization states is realized. Figure 3(a1) shows the theoretical result of the FF vectorial Taiji pattern. The arrows represent the polarization direction of the corresponding area. To verify the vectorial properties of the FF Taiji pattern, the corresponding experimental results are also measured which are shown in the second row of Fig. 3. As the generated Taiji pattern goes through a GT prism, the intensity changes as well as the GT prism rotates. Figures 3(a2)–3(a4) show the intensity profiles of the FF Taiji pattern in theory when the angle of the GT prism is $30°, 90°, 150°$ with respect to the positive horizontal direction. The corresponding experimental results are displayed in Figs. 3(b2)–3(b4). We can see that the intensity is isolated by the dark line, which is aroused by the phase jump between different parts and the diffraction effect of the optical field. It is noticeable that the intensity of the left part is higher when the polarization angle arrives at 90° as the polarization of the left part is in the vertical direction. On the contrary, the

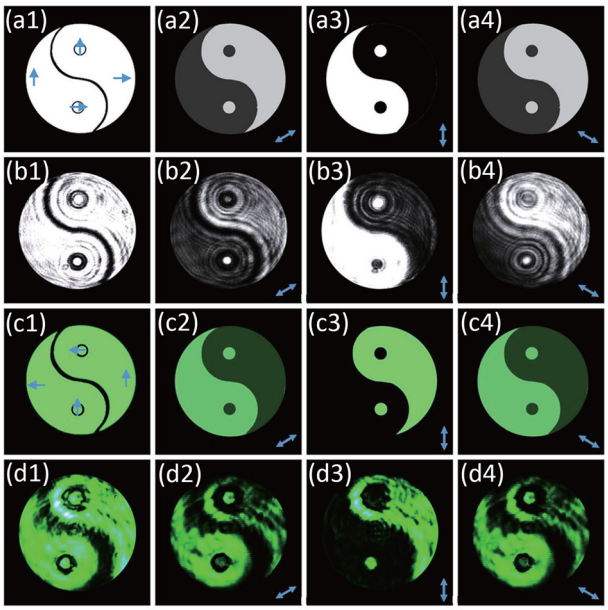


**FIG. 3.** (a1)–(a4) and (c1)–(c4) Show the simulated results of FF and SH Taiji pattern, respectively. Arrows in (a1) and (c1) show the polarization direction of the corresponding area. (b1)–(b4) and (d1)–(d4) Show the experimentally recorded intensity profile of the FF and SH Taiji patterns corresponding to the theoretical ones. Arrows in (a2)–(a4) and (c2)–(c4) show the polarization angles ($30°, 90°, 150°$) of the GT prism with respect to the positive horizontal direction.

right part shows a higher intensity as the right part component is larger while the polarization angle of the GT prism is 30° and 150°. Furthermore, the SH Taiji patterns are theoretically depicted in Figs. 3(c1)–4(c4) according to the nonlinear coupled wave equation. The corresponding experimental results are displayed in Figs. 3(d1)–4(d4). It is also worth noting that the polarization state of the identical SH Taiji part is perpendicular to that of the FF one, which is on account of the type-I (oo-e) phase matching process. As a result, the intensity of the left part of the SH Taiji pattern becomes weaker when the GT prism is rotated from 30° to 90° directions, whereas the intensity of the left part increases as the angle changes from 90° to 150°. The intensity alteration of the right part is contrary to the left one.

To better reveal the flexibility of the proposed method in the nonlinear field, a nonlinear vectorial clover pattern with three different polarization states is also generated. Figures 4(a) and 4(b) represent the FF and SH clover patterns in theory and the arrows show the polarization direction of the corresponding area. To better exhibit the vector properties of the nonlinear clover pattern, the background around the pattern that has different polarization directions is removed. Figures 4(c1) and 4(d1) show the simulated and experimental results of the generated SH clover pattern, respectively. As the lower one has a horizontal polarization, it is clear to see that the intensity of the lower leaf is much higher than those of the other two when the GT prism has a polarization angle of 0°. However, two wings are brighter than the lower one as the polarization angle of the GT prism is 90°, shown in Figs. 4(c4) and 4(d4). When the polarization angle of the GT prism is 45°, only the lower one left in Figs. 4(c3) and 4(d3), which is on account of the polarization direction of the two wings, is

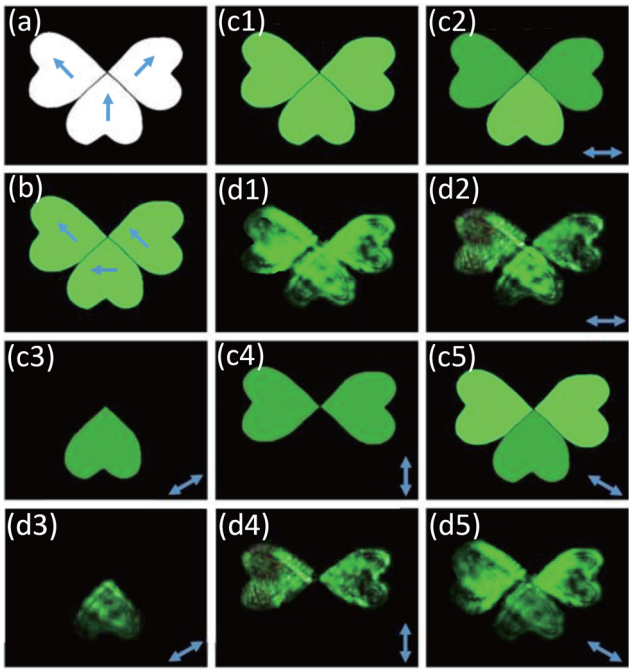


**FIG. 4.** (a) and (b) Show the simulated results of FF and SH clover patterns, respectively. Arrows in (a) and (b) show the polarization direction of the corresponding area. (d1)–(d5) Show the experimentally recorded intensity profile of the SH clover pattern corresponding to the theoretical ones (c1)–(c5). Arrows in (c2)–(c5) and (d2)–(d5) show the polarization angles ($0^\circ, 45^\circ, 90^\circ, 135^\circ$) of the GT prism with respect to the positive horizontal direction.

perpendicular to the polarization of the GT prism. With the polarization angle of 135°, the whole pattern emerges for no polarization state of the whole pattern is perpendicular to the polarization direction of the GT prism.

We would like to point out that the phase stabilization should be carefully solved in such a Mach–Zehnder interferometer when it is used to coherently combine optical fields in two separated arms. Fortunately, such stability issues can be effectively removed by using mature technology, which is commercially available. An air floated platform can be used as the optical table system to reduce the vibration. A plastic protective cover is also used to avoid the influence of the airflow. Furthermore, active locking can also be used to completely eliminate such stability issues. Compared to previous publications,[29,30] two arms in such a Mach–Zehnder interferometer enable the separated samples adjust flexibility. Most importantly, the method may broaden the generation of the vectorial vector beam in the ultrafast field since it is possible to control the phase delay in the two arms of the Mach–Zehnder interferometer, which previous configurations cannot afford.

In conclusion, we have realized the nonlinear frequency conversion of vectorial optical fields in a Mach–Zehnder interferometer. Two samples in separated arms of the Mach–Zehnder interferometer enable nonlinear processes occur in two perpendicular directions at the same time. The case of the FF vectorial optical fields with topological charge $l = 3$ is investigated in simulated and experimental conditions. The experimental results are coincident with the simulated ones. To illustrate the flexibility of this method, nonlinear Taiji and clover patterns with different polarization states are also generated. This study proposes a more flexible method to realize nonlinear frequency conversion of the vectorial optical fields and may have potential applications in the generation of ultrafast vectorial optical fields.

This work was supported in part by the National Key R&D Program of China under Grant Nos. 2018YFA0306300 and 2017YFA0303700, the National Natural Science Foundation of China (NSFC) under Grant No. 11734011, and The Foundation for Development of Science and Technology of Shanghai under Grant No. 17JC1400400.

## REFERENCES

[1]E. Snitzer, J. Opt. Soc. Am. **51**, 491 (1961).
[2]Y. Mushiake, K. Matsumura, and N. Nakajima, Proc. IEEE **60**, 1107 (1972).
[3]D. Pohl, Appl. Phys. Lett. **20**, 266 (1972).
[4]Q. Zhan and J. R. Leger, Opt. Express **10**, 324 (2002).
[5]Y. Zhao and J. Wang, Opt. Lett. **40**, 4843 (2015).
[6]R. Dorn, S. Qubis, and G. Leuchs, Phys. Rev. Lett. **91**, 233901 (2003).
[7]T. G. Brown, Prog. Opt. **56**, 81 (2011).
[8]C. Hnatovsky, V. G. Shvedov, and W. Krolikowski, Opt. Express **21**, 12651 (2013).
[9]M. Meier, V. Romano, and T. Feurer, Appl. Phys. A **86**, 329 (2007).
[10]C. Min, Z. Shen, J. Shen, Y. Zhang, H. Fang, G. Yuan, L. Du, S. Zhu, T. Lei, and X. Yuan, Nat. Commun. **4**, 2891 (2013).
[11]S. E. Skelton, M. Sergides, R. Saija, M. A. Iatì, O. M. Maragó, and P. H. Jones, Opt. Lett. **38**, 28 (2013).
[12]A. F. Abouraddy and K. C. Toussaint, Phys. Rev. Lett. **96**, 153901 (2006).
[13]G. Bautista and M. Kauranen, ACS Photonics **3**, 1351 (2016).
[14]Y. Chen and Y. Cai, Opt. Lett. **39**, 2549 (2014).
[15]X. Weng, L. Du, P. Shi, and X. Yuan, Opt. Express **25**, 9039 (2017).
[16]G. Bautista, J. Mäkitalo, Y. Chen, V. Dhaka, M. Grasso, L. Karvonen, H. Jiang, M. J. Huttunen, T. Huhtio, H. Lipsanen, and M. Kauranen, Nano Lett. **15**, 1564 (2015).
[17]B. Jia, X. Gan, and M. Gu, Opt. Express **13**, 6821 (2005).
[18]L. Huang, H. Guo, J. Li, L. Ling, B. Feng, and Z. Y. Li, Opt. Lett. **37**, 1694 (2012).
[19]J. Lin, K. Yan, Y. Zhou, L. X. Xu, C. Gu, and Q. W. Zhan, Appl. Phys. Lett. **107**, 191108 (2015).
[20]L. Gong, Y. Ren, W. Liu, M. Wang, M. Zhong, Z. Wang, and Y. Li, J. Appl. Phys. **116**, 183105 (2014).
[21]F. Yue, D. Wen, J. Xin, B. D. Gerardot, J. Li, and X. Chen, ACS Photonics **3**, 1558 (2016).
[22]A. Arbabi, Y. Horie, M. Bagheri, and A. Faraon, Nat. Nanotechnol. **10**, 937 (2015).
[23]P. Chen, Y. Lu, and W. Hu, Liq. Cryst. **43**, 2051 (2016).
[24]I. Moreno, M. M. Sanchez-Lopez, K. Badham, J. A. Davis, and D. M. Cottrell, Opt. Lett. **41**, 1305 (2016).
[25]P. Chen, W. Ji, B. Wei, W. Hu, V. Chigrinov, and Y. Lu, Appl. Phys. Lett. **107**, 241102 (2015).
[26]X. Wang, J. Ding, W. Ni, C. Guo, and H. Wang, Opt. Lett. **32**, 3549 (2007).
[27]X. Wang, Y. Li, J. Chen, C. Guo, J. Ding, and H. Wang, Opt. Express **18**, 10786 (2010).
[28]W. Han, Y. Yang, W. Cheng, and Q. Zhan, Opt. Express **21**, 20692 (2013).
[29]H. Liu, H. Li, Y. Zheng, and X. Chen, Opt. Lett. **43**, 5981 (2018).
[30]C. Yang, Z.-Y. Zhou, Y. Li, Y.-H. Li, S.-L. Liu, S.-K. Liu, Z.-H. Xu, G.-C. Guo, and B.-S. Shi, Opt. Lett. **44**, 219 (2019).
[31]O. Gayer, Z. Sacks, E. Galun, and A. Arie, Appl. Phys. B **91**, 343 (2008).